Neuron
Report

# Nanoscale Scaffolding Domains within the Postsynaptic Density Concentrate Synaptic AMPA Receptors

Harold D. MacGillavry,[1,2] Yu Song,[3] Sridhar Raghavachari,[4] and Thomas A. Blanpied[1,2,*]
[1]Department of Physiology
[2]Program in Neuroscience
University of Maryland School of Medicine, Baltimore, MD 21201, USA
[3]Department of Physics, Duke University
[4]Department of Neurobiology, Duke University Medical Center
Durham, NC 27710, USA
*Correspondence: tblanpied@som.umaryland.edu
http://dx.doi.org/10.1016/j.neuron.2013.03.009

## SUMMARY

**Scaffolding molecules at the postsynaptic membrane form the foundation of excitatory synaptic transmission by establishing the architecture of the postsynaptic density (PSD), but the small size of the synapse has precluded measurement of PSD organization in live cells. We measured the internal structure of the PSD in live neurons at approximately 25 nm resolution using photoactivated localization microscopy (PALM). We found that four major PSD scaffold proteins were each organized in distinctive ~80 nm ensembles able to undergo striking changes over time. Bidirectional PALM and single-molecule immunolabeling showed that dense nanodomains of PSD-95 were preferentially enriched in AMPA receptors more than NMDA receptors. Chronic suppression of activity triggered changes in PSD interior architecture that may help amplify synaptic plasticity. The observed clustered architecture of the PSD controlled the amplitude and variance of simulated postsynaptic currents, suggesting several ways in which PSD interior organization may regulate the strength and plasticity of neurotransmission.**

## INTRODUCTION

Postsynaptic scaffolding molecules establish the internal organization of the postsynaptic density (PSD), critically determining the characteristics of excitatory synaptic transmission. However, though extensive genetic, biochemical, and molecular analysis has provided a wealth of information as to the characteristics of individual constituents of the PSD (Sheng and Hoogenraad, 2007), it is unclear how these constituents are arranged in individual PSDs, and whether this organization is dynamically regulated in living synapses. A particularly important aspect of PSD organization is the subsynaptic positioning of AMPA-type glutamate receptors (AMPARs) (MacGillavry et al., 2011). Because only AMPARs very near a presynaptic release event are exposed to a sufficiently high concentration of glutamate to become activated, the local density of receptors apposing the release site ultimately determines the strength of a synaptic response (Franks et al., 2003; Lisman et al., 2007; Raghavachari and Lisman, 2004). Furthermore, receptors are not uniformly distributed within the PSD but are commonly immobile and confined within subsynaptic domains (Ehlers et al., 2007; Heine et al., 2008; Kerr and Blanpied, 2012). Understanding mechanisms that underlie subsynaptic positioning of AMPARs and the scaffolding molecules that bind them within individual PSDs is thus critical for a better understanding of synaptic transmission. Even more broadly, however, the subsynaptic positioning of other scaffold-linked components of the PSD, such as adhesion molecules, signaling intermediates, and the cytoskeleton, control diverse aspects of synaptic function and plasticity.

Directly determining the structural organization of the PSD in living neurons has been technically challenging because the small dimensions of the synapse essentially lie beyond the resolution of conventional optical imaging. As a result, our current understanding of the structural organization of the PSD is mainly derived from studies on biochemically isolated PSDs or fixed-tissue microscopy, culminating in the assumption that the PSD is a homogeneous and static structure. In contrast, live-cell microscopy revealed that the PSD is a very dynamic structure with individual components continuously being repositioned (Blanpied et al., 2008; Kerr and Blanpied, 2012) and exchanged (Kuriu et al., 2006; Sturgill et al., 2009). Here, we have used live-cell superresolution photoactivated localization microscopy (PALM) (Betzig et al., 2006; Hess et al., 2006) to map the spatial distribution of molecular families within single PSDs at nanometer resolution and resolve the dynamic interior organization of living synapses. We find that scaffold proteins in individual PSDs are not homogeneously distributed but rather accumulate in dense, subsynaptic clusters and that PSD-95-dense scaffold domains are preferentially enriched in AMPARs.

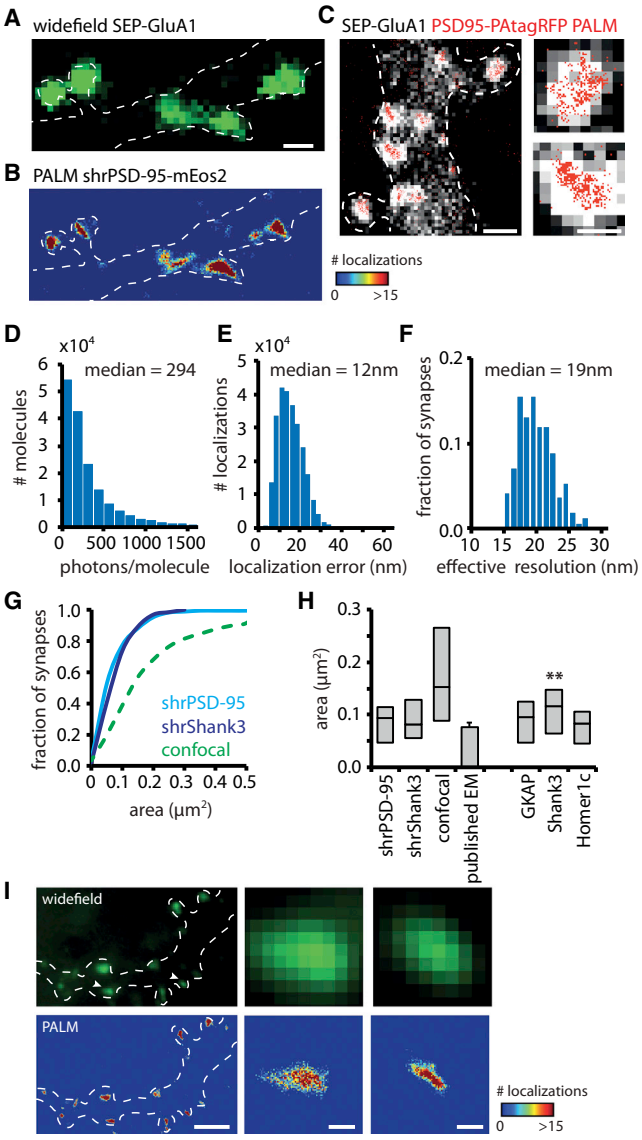


**Figure 1. Superresolution Imaging of the Postsynaptic Density**

(A) Oblique illumination of SEP-GluA1 marking synapses along a stretch of dendrite, 100 nm pixels. (B) Same region, PALM image of shrPSD-95-mEos2, 25 nm pixels. Scale bar represents 500 nm. (C) Single-molecule localizations of PSD-95-PAtagRFP PALM (red) superimposed upon the widefield image of SEP-GluA1 fluorescence (white). Scale bars represent 1 μm (left) and 500 nm (right). (D and E) Histograms of number of detected photons per molecule (D) and localization precision (E). (F) Histogram of effective resolution calculated from the localization precision and density of shrPSD-95-mEos2 molecules in individual PSDs. (G) Cumulative distribution of PSD area measured by PALM for mEos2-tagged shrPSD-95 and shrShank3 compared with confocal microscopy of neurons expressing shrPSD-95-GFP. (H) Boxplot summary of PSD area measured by PALM for shrPSD-95 and shrShank3, compared with confocal, mean PSD area based on published EM data (see Results) and PALM on neurons overexpressing GKAP, Shank3, or Homer1c. **$p < 0.01$, Kruskal-Wallis. (I) Comparison of summed oblique illumination (top) and PALM image (bottom) of shrPSD-95-mEos2. Arrowheads mark PSDs expanded at right. Pixel size is 25 nm (left) and 12 nm (right). Scale bar represents 2.5 μm (left) and 200 nm (right).

## RESULTS

### Live-Cell Superresolution Imaging of the Postsynaptic Density

To study the subsynaptic distribution of PSD-95 using live-cell PALM, we transfected rat hippocampal neurons in dissociated culture with a PSD-95 replacement construct (shrPSD-95; see Figures S1A–S1C available online) tagged with mEos2. Individual molecules were stochastically activated using weak 405 nm illumination and excited during 50 Hz imaging with oblique illumination at 561 nm (Frost et al., 2010b). Compared to wide-field images, PALM revealed sharper images of PSDs that were clearly delineated by an abrupt drop in scaffold molecule density at the PSD edge (Figures 1A and 1B). PSD-95 molecules colocalized with clustered cell-surface AMPARs (Figure 1C). We estimated the effective map resolution to be ~25 nm, based on the localization precision (<15 nm) and the density of localizations within individual PSDs (Figures 1D–1F, S1D–S1F).

We analyzed PSD morphology by thresholding the PALM density maps to outline individual PSDs (Figure S1G). PSD area measured with PALM ranged from 0.02 to 0.53 $\mu m^2$ (0.094 ± 0.005 $\mu m^2$, mean ± SEM, n = 169/20 PSDs/neurons), significantly lower than measures based on confocal microscopy (0.226 ± 0.008 $\mu m^2$, n = 810/3), and approaching the reported range of PSD area of in vivo hippocampal CA1 synapses measured by serial section electron microscopy (EM) (from 0.008 to 0.54 $\mu m^2$, mean: 0.069 $\mu m^2$) (Harris and Stevens, 1989; Schikorski and Stevens, 1997; Shinohara et al., 2008) (Figures 1G and 1H). No differences in PSD area were noted between spine and shaft synapses (Figures S1I and S1J). PSD area was well correlated with the absolute number of localizations within the PSD, but not with the density of localizations (Figures S1K and S1L). The counted number of localizations per PSD (median, 609) overestimates the number of synaptic PSD-95 molecules because of overexpression (1.6-fold, Figure S1B) and additionally as a consequence of blinking fluorophores (as described below). When corrected for these factors, the number of PSD-95 molecules per PSD is estimated to be ~300, in line with previous estimates (Chen et al., 2008; Sugiyama et al., 2005).

PSD area was similar based on PALM imaging in neurons expressing a Shank3 replacement construct (shrShank3-mEos2; 0.094 ± 0.005 $\mu m^2$, n = 121/11), as well as in neurons overexpressing GKAP-mEos2 (0.095 ± 0.006 $\mu m^2$, n = 110/18) or Homer1c-mEos2 (0.083 ± 0.003 $\mu m^2$, n = 210/12). However, PSDs in neurons overexpressing Shank3-mEos2 were larger (0.12 ± 0.006 $\mu m^2$, n = 196/24; Figure 1H), emphasizing the importance of the replacement approach. Morphologies of individual PSDs were highly diverse, often with complex, irregular borders (Figures 1I). In sum, these observations indicate that PALM reliably measures living synapses with unprecedented clarity, revealing detailed structural features unresolved by confocal microscopy.

### Subsynaptic Pattern of Scaffold Molecules in Individual Synapses Is Not Homogenous

To visualize the distribution of individual scaffold molecules within the PSD, we plotted measured locations and color coded them according to their local density (Figures 2A and 2B). We

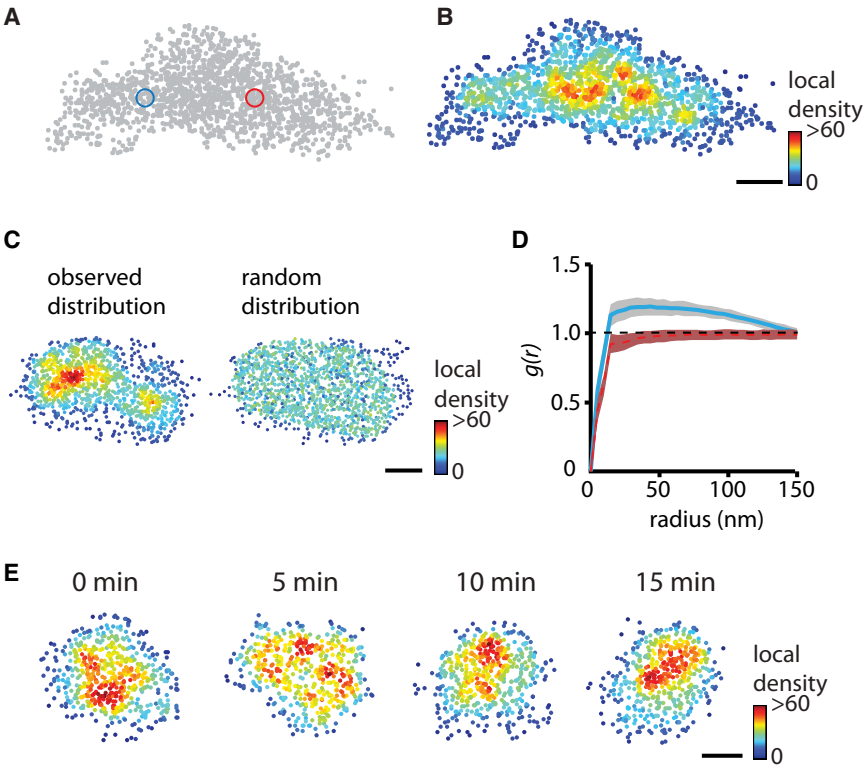


**Figure 2. Heterogeneous Distribution of Scaffold Molecules within the Postsynaptic Density**

(A and B) Single-molecule localization of PSD-95-Eos2. Individual molecules were color coded according to their local density (B), and the number of molecules within a radius five times the average nearest neighbor distance within the PSD (blue and red circles). Scale bar represents 100 nm. (C) Homogenous distribution (right) generated by randomly sampling equal numbers of localizations as observed (left). Scale bar represents 100 nm. (D) Mean pair-correlation function of the PSD in (C) for the measured particle locations (blue) and for the simulated locations (red). Shaded areas represent 99% confidence intervals calculated from the randomized ensembles, showing significant departures from homogeneity. (E) Example of a time series of shrPSD-95-mEos2 local density plots, revealing time-dependent variation in the distribution of PSD-95 molecules within the PSD. Scale bar represents 100 nm.

calculated the local density $D_L$ around each molecule by counting the number of neighbors within a radius scaled to the mean density in its PSD. This strategy accounts for variation in the copy number of scaffolds in each synapse and the number of localizations achieved per PSD. Typically, the scaling radius was ~30 nm (see Supplemental Experimental Procedures for details) and thus samples the immediate environment of the molecule. This analysis resulted in fine-scale maps of the local molecular density of individual synapses and revealed a highly nonuniform distribution of PSD-95 molecules in single PSDs (Figure 2B).

To test whether the observed distributions exhibited structure beyond that expected to occur in random distributions of points, we used pair-correlation functions (PCFs; see Supplemental Experimental Procedures for details). The measured PCF showed significant inhomogeneity compared to randomly generated ensembles (Figure 2D) for 65% of all PSDs ($p < 0.001$). Furthermore, the median distance over which the distribution was significantly more dense than random was ~70 nm, suggestive of clustering of scaffold molecules over this length scale within the PSD. Extensive simulations of PSDs on surfaces with varying degrees of roughness and subjected to random orientations furthermore suggested that the clusters we observed did not arise because of curvature or complexity of the synaptic membrane, or because of the orientation of the PSD relative to the imaging plane (Figure S2).

The measured distribution of PSD-95 varied greatly between synapses, which could reflect either inherent structural differences among individual PSDs or time-variant reorganization in single synapses. To distinguish between these possibilities, we acquired PALM images every 5 min from live neurons. The distribution pattern of PSD-95 differed greatly between consecutive time points (Figure 2E), suggesting that internal PSD structure was continuously reorganizing. Single-molecule tracking revealed that individual scaffold molecules moved at velocities below our level of detection (data not shown), consistent with their confinement within small subdomains of the PSD matrix (Kerr and Blanpied, 2012). This suggests that the continuously shifting distribution reflects a local reorganization of constituents rather than movement over longer distances within the synapse. Nevertheless, morphing or three-dimensional rotation of the PSD probably influenced our measured cluster dynamics as well. The magnitude of this influence is difficult to test experimentally but appears low. However, our simulations (Figure S2) suggest that only extreme deformation of overall PSD structure could alter the measured PSD-95 distribution to an extent approaching what we observed in live cells. Together, these considerations are consistent with the conclusion that regions of high local scaffold density undergo substantial changes over time.

## Scaffold Molecules Are Organized in Subsynaptic Clusters

In most synapses, scaffold molecules were enriched in one or two distinctive clusters (Figures 3A and 3B). To delineate these, we defined criteria by using a Monte Carlo approach to simulate random molecule locations within an elliptic region resembling an average synapse and by varying the simulated molecular density, localization precision, and amount of fluorophore blinking (Figure S3). These simulations resulted in a set of objective criteria that reliably defined the borders of simulated clusters (Figure S3). Note, however, that in order to avoid false positives, this conservative procedure reduces identification of genuine clusters that are small or contain few localized molecules. Using these criteria, we found that 70% of the PSDs were defined as

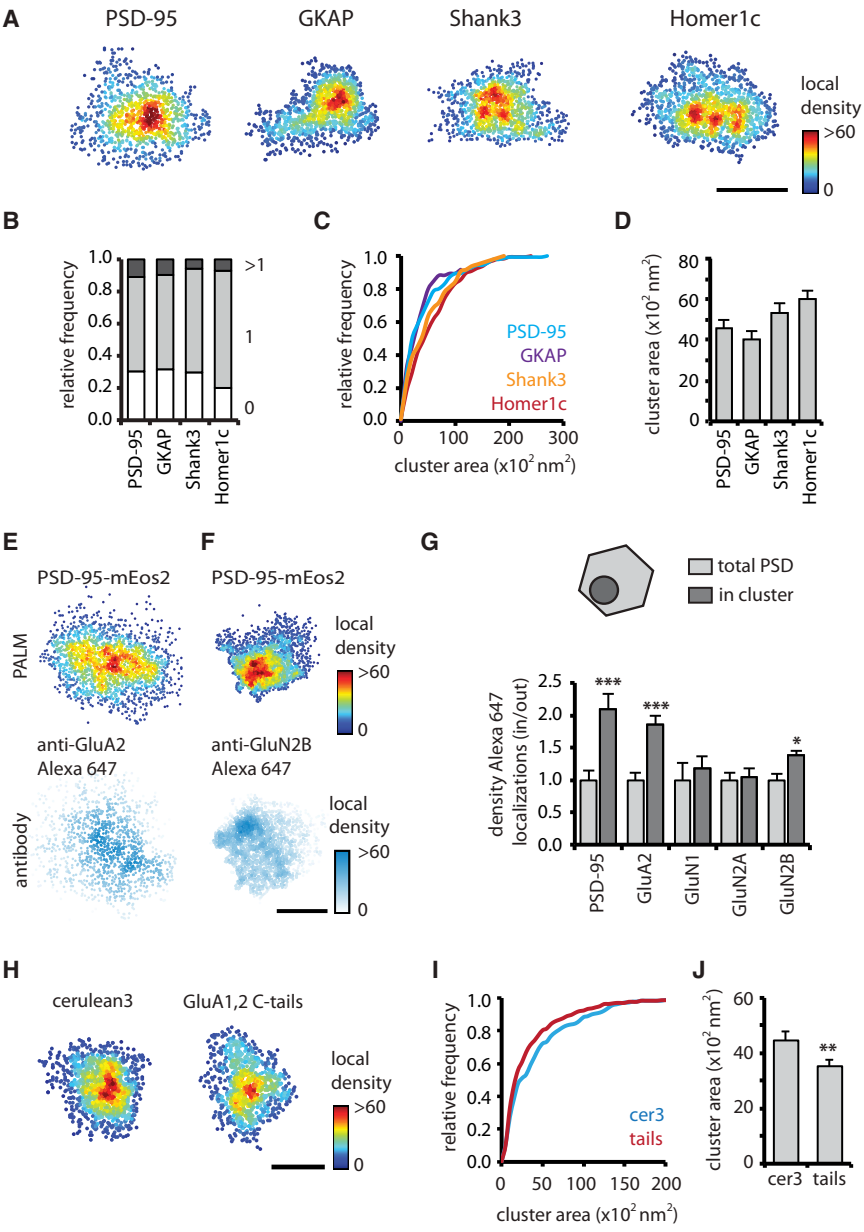


**Figure 3. Scaffold Organization in Subsynaptic Clusters Enriched in AMPARs**

(A) Examples of PSDs resolved with PALM for mEos2-tagged shrPSD-95, GKAP, shrShank3, and Homer1c. Scale bar represents 200 nm. (B) Relative frequency of PSDs with 0, 1, or more clusters. (C and D) Cumulative frequency distribution (C) and mean of cluster area (D) for different scaffold molecules. (E and F) Examples of two-color single-molecule imaging for shrPSD-95-mEos2 and GluA2 (E) or GluN2B (F). Scale bar represents 200 nm. (G) Relative enrichment of PSD-95, GluA2, GluN1, GluN2A, and GluN2B localizations inside and outside of subsynaptic PSD-95 clusters. Alexa 647 localizations within the PSD defined by PSD-95-mEos2 (polygonal) were extracted, and the densities in and out of the subdomain (circle) were compared. ***$p < 0.001$, *$p < 0.05$, two-way ANOVA with Bonferroni post hoc test. (H) Examples of PSDs resolved with PALM in cerulean3 or GluA1,2 C-tail expressing neurons. (I and J) Cumulative frequency distribution and mean of cluster area for control (cer3) and GluA1,2 C-tail (tails) expressing neurons. **$p < 0.01$, different from control, Kolmogorov-Smirnov test. All error bars represent SEM.

containing subclusters. Roughly similar percentages of PSDs expressing tagged GKAP, Shank3, or Homer1c contained one or more clusters (Figure 3B). The area of measured PSD-95 subclusters was 4,580 ± 402 nm$^2$ (diameter: 83 ± 4 nm). On average, 17% ± 1% of the molecules in the PSD resided in these clusters, with a resulting density 3.6 ± 0.1 times higher than the overall density in the PSD. We observed similar measures for the other scaffold molecules (Figures 3C and 3D), illuminating an unforeseen level of subsynaptic organization.

## Subsynaptic Scaffolding Domains Concentrate Synaptic AMPARs

To test whether NMDA or AMPA-type glutamate receptors are enriched in subsynaptic scaffold clusters, we used two-color, single-molecule imaging on neurons transfected with shrPSD-95-mEos2 and stained for GluA2-containing AMPARs or GluN1-, GluN2A-, and GluN2B-containing NMDARs. Images of photoswitched mEos2 and Alexa 647-conjugated antibodies were acquired simultaneously, localized, and overlaid (Figures 3E and 3F, S3J and S3L). Alexa 647 localizations within the borders of PSDs were extracted. The distribution of receptors was distinctively heterogeneous, containing notable peaks within the PSD border, consistent with previous superresolution imaging (Dani et al., 2010). To examine the relative enrichment in subsynaptic scaffold domains, we analyzed PSD-95 local density maps for subclusters as above, and we compared the density of Alexa 647 localizations inside and outside of these domains (Figure 3G). Importantly, subcluster area measured by PALM in fixed and live cells was similar (fixed: 4,462 ± 333 nm$^2$; live: 4,580 ± 402 nm$^2$), indicating that fixation did not alter PSD substructure (and that ongoing dynamics of PSD structure did not substantially affect our live-cell measurements). We found that the relative density of GluA2 localizations within clusters was significantly higher than in the entire PSD (relative density: 1.9 ± 0.1, n = 57/11). In contrast, GluN1 (1.2 ± 0.2, n = 61/8) and GluN2A (1.0 ± 0.1, n = 64/15) localizations were not enriched. Interestingly, though, there was a modest enrichment of GluN2B localizations (1.4 ± 0.1, n = 74/8). Note that we cannot be certain that we stained surface receptors only. However, although recycling organelles

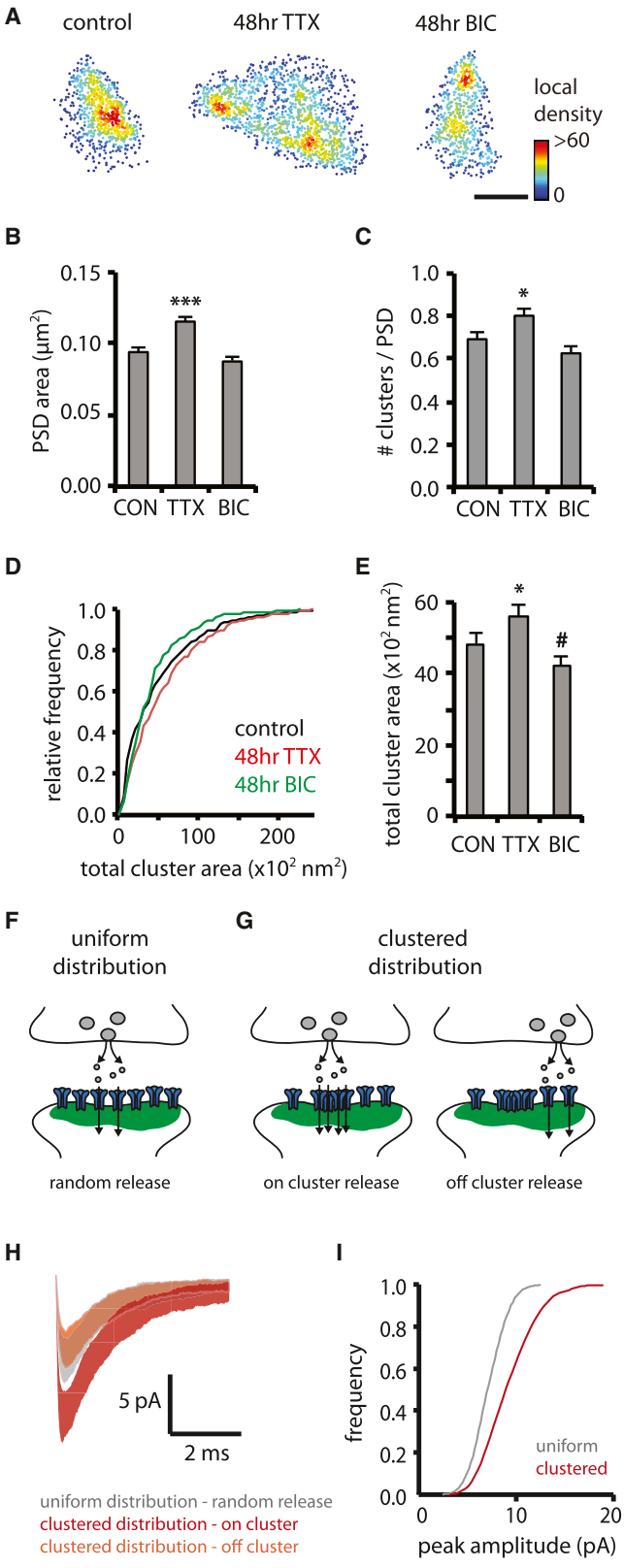


**Figure 4. Subsynaptic Structure Is Altered by Synaptic Activity and Shapes Postsynaptic Responses**

(A) Examples of PSDs resolved with PALM comparing a control PSD with PSDs after chronic treatment with TTX or bicuculline (BIC). Scale bar represents 200 nm. (B) Mean PSD area for control, TTX, and BIC treatment. ***$p < 0.001$, Kruskal-Wallis. (C) Mean number of clusters per PSD for control, TTX, and BIC. *$p < 0.05$, one-way ANOVA. (D and E) Cumulative frequency distribution (D) and mean of total cluster area (E) for control, TTX, and BIC. *$p < 0.05$, different from control, #$p < 0.1$, K-S test. All error bars represent SEM. (F and G) Postsynaptic currents were simulated assuming randomly positioned release events on a uniform distribution of AMPARs (F), compared with release on and outside of a subsynaptic cluster of the AMPAR distribution measured in Figure 3E (G). (H) Average mEPSC trace ± SD of 50 runs for uniform distribution with random release locations compared with on and off cluster release for the clustered distribution. (I) Cumulative frequency distribution of peak amplitude for simulated mEPSCs comparing randomly positioned release events (50 runs/location, 50 locations) on a uniform or clustered distribution of AMPARs.

potentially containing receptors are found in approximately half of spines at rest (Park et al., 2006), they are rarely found directly under the synapse, where they could be confused with the PSD. By analyzing only localizations within the border of the PSD, we were able to exclude the majority of internal receptors from our analysis. In control experiments, we found enrichment of PSD-95 immunolabeled molecules within clusters identified via shrPSD-95-mEos2 PALM (2.1 ± 0.2, n = 19/3; Figure 3G). Additionally, expressed GluA2-mEos3.2 localized by PALM was enriched in clusters defined by immunolabeling of endogenous PSD-95 (2.1 ± 0.3, n = 27/10).

AMPAR enrichment within scaffold subdomains may reflect a role for receptors in creating clusters. To test whether a downregulation of synaptic AMPARs reduces subsynaptic scaffold clustering, we expressed shrPSD-95-mEos2 along with GluA1 and GluA2 C-terminal domains ("GluA tails") previously shown to reduce synaptic levels of AMPARs (Shi et al., 2001) but not PSD-95 (Ripley et al., 2011). Interestingly, while expression of the GluA tails did not alter either PSD area (control, 0.093 ± 0.004 $\mu m^2$; tails, 0.087 ± 0.003 $\mu m^2$, n = 264/17 and 430/24 respectively, p = 0.21) or the fraction of clustered PSDs (control, 59%; tails, 61%), the area of subsynaptic scaffolding domains was substantially and significantly decreased in neurons expressing GluA tails (control: 4,446 ± 352 $nm^2$; tails: 3,522 ± 21 $nm^2$, Figures 3H–3J).

## Homeostatic Scaling of Synaptic Substructure

Chronic changes in network activity result in the homeostatic scaling of synaptic strength, which involves a bidirectional change in miniature excitatory postsynaptic current (mEPSC) amplitude and synaptic AMPAR abundance. We tested whether long-term activity blockade or elevation changes PSD morphology or substructure. Activity blockade with TTX for 2 days significantly increased PSD area (control: 0.094 ± 0.003 $\mu m^2$; TTX: 0.125 ± 0.004 $\mu m^2$, n = 454/18 and 332/20, respectively), while elevation of network activity with bicuculline showed a trend to reduce PSD area (0.088 ± 0.003 $\mu m^2$, n = 329/11, Figures 4A and 4B). Importantly, by examining PSD interior organization, we found that TTX significantly increased the average number of subsynaptic scaffold clusters per synapse (control: 0.69 ± 0.03; TTX: 0.80 ± 0.04), as well as the total

area per PSD in which PSD-95 was clustered (control: 4,842 ± 298 nm$^2$; TTX: 5,616 ± 329 nm$^2$) (Figures 4C–4E).

### Clustered Distribution Shapes Postsynaptic Responses

To test the physiological impact of the observed nonuniform distribution of AMPARs on the size and variability of postsynaptic currents, we used Monte Carlo simulations of receptor activation after release of a single vesicle of glutamate in a structurally constrained model of the synapse (Raghavachari and Lisman, 2004; Santucci and Raghavachari, 2008). We simulated release over a uniform distribution of AMPARs or a clustered distribution derived from the measured GluA2 locations in Figure 3E (Figure 4G). We found that mEPSC amplitudes resulting from a release event on a cluster of AMPARs were much larger (~2-fold, $p < 0.001$) than responses to "off-cluster" release or randomly localized release on a uniform distribution (~1.5-fold, $p < 0.001$; Figure 4H). Simulations of responses to randomly released vesicles across the entire face of the PSD showed that the distribution of mEPSC peak amplitudes exhibited larger amplitude (median = 10 pA) and coefficient of variation (0.50) for a clustered arrangement of receptors compared to a uniform distribution (median = 7 pA, CV = 0.35, $p < 0.001$).

## DISCUSSION

Using a combination of live-cell, single-molecule imaging and quantitative spatial analysis, we have examined PSD morphology and substructure at substantially improved resolution (~25 nm). Direct measurements of the distribution of individual molecules across the dimensions of the synapse revealed a structured pattern of scaffold molecules enriched in subsynaptic, nanometer-scale domains. Averaging ~80 nm in diameter, these domains contained 15%–20% of the scaffold content of the synapse, packed at roughly three times the density of the remainder of the PSD. Thus, PSD assembly from individual constituents results in emergent structural features incorporating dozens or hundreds of proteins.

Four major classes of scaffold proteins each were clustered. While we have not measured the spatial relation between different scaffolds within individual PSDs, it is conceivable that through their interactions, different scaffold proteins accumulate in the same or interlinked domains. Immunogold EM has in general reported no systematic density variation across the synapse (Valtschanoff and Weinberg, 2001); however, from analysis of biochemically isolated PSDs, PSD-95 distribution was found to be nonuniform (DeGiorgis et al., 2006; Swulius et al., 2010). In addition, recent immunolabeling STORM indeed revealed a high variability in protein distribution between individual synapses (Dani et al., 2010). Our live-cell approach extends this notion in that the pattern of scaffold positioning within the PSD not only varies greatly between synapses but also undergoes robust changes over time.

GluA2-containing AMPARs were enriched in subsynaptic domains dense in PSD-95. This is consistent with the notion that the interaction of AMPARs with PSD-95 via TARPs is required for subsynaptic receptor positioning, just as it is for the overall retention of AMPARs in synapses (Bats et al., 2007; Chen et al., 2000). Indeed, measurements via confocal microscopy have noted a very high spatial correlation in single synapses between AMPARs and PSD-95 (Kerr and Blanpied, 2012). The high mobility and exchange rate of AMPARs (Heine et al., 2008) suggest that they do not themselves dictate the fine-scale distribution of synaptic scaffolds. However, we found that reduction of AMPAR content via GluA C-tail expression reduced cluster size, whereas TTX treatment, known to increase AMPAR number, increased cluster size. Together, these results suggest that scaffold proteins probably establish the architectural basis for clustering but that receptor molecules participate as well. Other mechanisms such as macromolecular crowding (Santamaria et al., 2010) may in addition serve synergistically to maintain elevated receptor density in clustered subregions of the PSD.

Though many GluN2B-containing receptors lie extrasynaptically, we found that those in the synapse are moderately enriched in PSD-95-rich domains. Previous modeling has shown that the activation of GluN2B-containing receptors after vesicular release drops off quickly away from the site of release, owing to slow receptor activation kinetics (Santucci and Raghavachari, 2008). Thus, concentration of GluN2B receptors in scaffold domains away from the edge of the synapse may serve to increase their relative probability of opening. In addition, as the GluN2B subunit is the dominant PSD binding site for active CaMKII, it seems likely that substrates within the cluster, such as AMPARs, TARPs, or GKAP, may be targeted preferentially for phosphorylation, refining the modulation of synaptic strength by activity (Lisman et al., 2012).

In our simulations, we observed that glutamate release over clustered receptors evoked EPSCs nearly twice as large as elsewhere in the PSD. Concentrating AMPARs near sites of release is thus a powerful means to maximize the efficiency of synaptic transmission and clusters of PSD-95 would provide a natural epicenter of pre-post alignment to maximize this effect. For instance, PSD-95 may seed the distribution of adhesion molecules that influence presynaptic organization. Alternatively, the AMPAR N-terminal domain could provide a direct transsynaptic link to coordinate alignment with release sites (Saglietti et al., 2007). Active zone structure is complex and heterogeneous, with calcium channels perhaps loosely clustered (Holderith et al., 2012) and other components of the presynaptic cytomatrix appearing in repeating groups, potentially dictating release sites (Burette et al., 2012). It may be that dense scaffold domains, which tend to be more central than at the border of PSDs, help principally to congregate receptors toward the center of the synapse rather than specifically align them with release sites. Indeed, release at randomly distributed sites still evoked much larger mean EPSCs at clustered PSDs than those with the same number of receptors uniformly distributed. However, suggestions that release mode (Park et al., 2012) and spontaneous versus action potential-evoked fusion (Kavalali et al., 2011) may influence subsynaptic release location highlight the importance of understanding mechanisms that transsynaptically match active zone and PSD organization.

Our observations suggest that modifying cluster size, position, or receptor content may magnify or diminish transmission, even in the absence of altered receptor number. Reorganization of scaffold ensembles in the absence of plasticity-inducing

stimuli suggests subsynaptic alignment is far from static even under basal conditions, further emphasizing recent observations that the PSD interior is a dynamic structure (Bats et al., 2007; Kerr and Blanpied, 2012). However, molecular destabilization of the PSD is prominent during induction of LTP and LTD (Steiner et al., 2008; Xu et al., 2008), suggesting that periods of plasticity involve substantially enhanced reorganization of the internal scaffold distribution. We speculate that the increased number and enlargement of PSD subclusters that we observed during activity blockade augments the influence of added AMPARs.

Distinct from effects on receptors, scaffold clusters deep in the PSD would be expected to influence postsynaptic signaling in many ways. Clusters of Shank probably determine points of attachment to the actin cytoskeleton through actin-binding proteins that interact with Shank (Haeckel et al., 2008; Naisbitt et al., 1999). Indeed, actin filaments contact the PSD at its interior face (Burette et al., 2012; Frost et al., 2010b). This contact may be critical for numerous steps in synaptic structural and functional plasticity (Frost et al., 2010a; Kerr and Blanpied, 2012), including the reorganization of scaffold patterning that we have observed here. Consistent with this idea, acute depolymerization of actin by latrunculin A reduced the area of PSD-95 clusters (Figure S4). Speculating more broadly, the distinctive, nanoscale organization of spine actin (Frost et al., 2010b; Urban et al., 2011) and the regulated positioning of perisynaptic receptor trafficking machinery (Blanpied et al., 2002; Kennedy et al., 2010) suggest that the actin cytoskeleton may tie the diverse regulatory components of the spine together into a functionally coordinated ensemble. It will thus be important to assess whether mechanisms that create or maintain the synaptic scaffold pattern also contribute to activity-dependent changes in spine structure, as disruption of these mechanisms may well lead to pathological synaptic dysfunction (Penzes et al., 2011; Ting et al., 2012). Continual improvement in superresolution imaging (Dani et al., 2010), particularly in live cells, should help to clarify the structural and molecular mechanisms in spines that establish and modulate synapse function.

## EXPERIMENTAL PROCEDURES

See Supplemental Experimental Procedures for details.

Dissociated hippocampal neurons from embryonic day 18 rat were prepared as described in Frost et al. (2010b). Cells were transfected 12–16 days after plating and imaged by oblique illumination PALM 72 hr later. Molecules were localized and assembled in density maps from which individual PSDs were delineated. Localizations within the borders of the PSD were then coded on the basis of their local density, and these maps were segmented to define subsynaptic clusters. For two-color, single-molecule imaging, PSD-95 or receptors were immunolabeled with Alexa 647-conjugated secondary antibodies. Images of photoswitched shrPSD-95-mEos2 and Alexa 647 molecules were acquired simultaneously, drift corrected, and aligned. Homeostatic scaling was induced by incubating cultures with TTX or bicuculline for 48 hr. mEPSCs were simulated as described (Raghavachari and Lisman, 2004).

## SUPPLEMENTAL INFORMATION

Supplemental Information includes four figures and Supplemental Experimental Procedures and can be found with this article online at http://dx.doi.org/10.1016/j.neuron.2013.03.009.

## ACKNOWLEDGMENTS

We would like to thank Scott Thompson, John Lisman, and members of the Blanpied Laboratory for helpful discussions and critical evaluation of the manuscript, Nick Frost for help designing the microscope and analysis software, and Tamar Davis and Minerva Contreras for excellent technical support. This work was supported by the NIH (MH080046 to T.A.B. and CRCNS grants MH096376 and DA027807 to S.R.), the Dana Foundation (to T.A.B.), the Broad Foundation (to S.R. and T.A.B.), and the Katherine D. and Theodore J. Carski Fund (to T.A.B.).

Accepted: March 8, 2013
Published: May 22, 2013

## REFERENCES

Bats, C., Groc, L., and Choquet, D. (2007). The interaction between Stargazin and PSD-95 regulates AMPA receptor surface trafficking. Neuron *53*, 719–734.

Betzig, E., Patterson, G.H., Sougrat, R., Lindwasser, O.W., Olenych, S., Bonifacino, J.S., Davidson, M.W., Lippincott-Schwartz, J., and Hess, H.F. (2006). Imaging intracellular fluorescent proteins at nanometer resolution. Science *313*, 1642–1645.

Blanpied, T.A., Scott, D.B., and Ehlers, M.D. (2002). Dynamics and regulation of clathrin coats at specialized endocytic zones of dendrites and spines. Neuron *36*, 435–449.

Blanpied, T.A., Kerr, J.M., and Ehlers, M.D. (2008). Structural plasticity with preserved topology in the postsynaptic protein network. Proc. Natl. Acad. Sci. USA *105*, 12587–12592.

Burette, A.C., Lesperance, T., Crum, J., Martone, M., Volkmann, N., Ellisman, M.H., and Weinberg, R.J. (2012). Electron tomographic analysis of synaptic ultrastructure. J. Comp. Neurol. *520*, 2697–2711.

Chen, L., Chetkovich, D.M., Petralia, R.S., Sweeney, N.T., Kawasaki, Y., Wenthold, R.J., Bredt, D.S., and Nicoll, R.A. (2000). Stargazin regulates synaptic targeting of AMPA receptors by two distinct mechanisms. Nature *408*, 936–943.

Chen, X., Winters, C., Azzam, R., Li, X., Galbraith, J.A., Leapman, R.D., and Reese, T.S. (2008). Organization of the core structure of the postsynaptic density. Proc. Natl. Acad. Sci. USA *105*, 4453–4458.

Dani, A., Huang, B., Bergan, J., Dulac, C., and Zhuang, X. (2010). Superresolution imaging of chemical synapses in the brain. Neuron *68*, 843–856.

DeGiorgis, J., Galbraith, J., Dosemeci, A., Chen, X., and Reese, T. (2006). Distribution of the scaffolding proteins PSD-95, PSD-93, and SAP97 in isolated PSDs. Brain Cell Biol. *35*, 239–250.

Ehlers, M.D., Heine, M., Groc, L., Lee, M.C., and Choquet, D. (2007). Diffusional trapping of GluR1 AMPA receptors by input-specific synaptic activity. Neuron *54*, 447–460.

Franks, K.M., Stevens, C.F., and Sejnowski, T.J. (2003). Independent sources of quantal variability at single glutamatergic synapses. J. Neurosci. *23*, 3186–3195.

Frost, N.A., Kerr, J.M., Lu, H.E., and Blanpied, T.A. (2010a). A network of networks: cytoskeletal control of compartmentalized function within dendritic spines. Curr. Opin. Neurobiol. *20*, 578–587.

Frost, N.A., Shroff, H., Kong, H., Betzig, E., and Blanpied, T.A. (2010b). Single-molecule discrimination of discrete perisynaptic and distributed sites of actin filament assembly within dendritic spines. Neuron *67*, 86–99.

Haeckel, A., Ahuja, R., Gundelfinger, E.D., Qualmann, B., and Kessels, M.M. (2008). The actin-binding protein Abp1 controls dendritic spine morphology and is important for spine head and synapse formation. J. Neurosci. *28*, 10031–10044.

Harris, K.M., and Stevens, J.K. (1989). Dendritic spines of CA 1 pyramidal cells in the rat hippocampus: serial electron microscopy with reference to their biophysical characteristics. J. Neurosci. *9*, 2982–2997.

Heine, M., Groc, L., Frischknecht, R., Béïque, J.C., Lounis, B., Rumbaugh, G., Huganir, R.L., Cognet, L., and Choquet, D. (2008). Surface mobility of postsynaptic AMPARs tunes synaptic transmission. Science *320*, 201–205.

Hess, S.T., Girirajan, T.P., and Mason, M.D. (2006). Ultra-high resolution imaging by fluorescence photoactivation localization microscopy. Biophys. J. *91*, 4258–4272.

Holderith, N., Lorincz, A., Katona, G., Rózsa, B., Kulik, A., Watanabe, M., and Nusser, Z. (2012). Release probability of hippocampal glutamatergic terminals scales with the size of the active zone. Nat. Neurosci. *15*, 988–997.

Kavalali, E.T., Chung, C., Khvotchev, M., Leitz, J., Nosyreva, E., Raingo, J., and Ramirez, D.M. (2011). Spontaneous neurotransmission: an independent pathway for neuronal signaling? Physiology (Bethesda) *26*, 45–53.

Kennedy, M.J., Davison, I.G., Robinson, C.G., and Ehlers, M.D. (2010). Syntaxin-4 defines a domain for activity-dependent exocytosis in dendritic spines. Cell *141*, 524–535.

Kerr, J.M., and Blanpied, T.A. (2012). Subsynaptic AMPA receptor distribution is acutely regulated by actin-driven reorganization of the postsynaptic density. J. Neurosci. *32*, 658–673.

Kuriu, T., Inoue, A., Bito, H., Sobue, K., and Okabe, S. (2006). Differential control of postsynaptic density scaffolds via actin-dependent and -independent mechanisms. J. Neurosci. *26*, 7693–7706.

Lisman, J.E., Raghavachari, S., and Tsien, R.W. (2007). The sequence of events that underlie quantal transmission at central glutamatergic synapses. Nat. Rev. Neurosci. *8*, 597–609.

Lisman, J.E., Yasuda, R., and Raghavachari, S. (2012). Mechanisms of CaMKII action in long-term potentiation. Nat. Rev. Neurosci. *13*, 169–182.

MacGillavry, H.D., Kerr, J.M., and Blanpied, T.A. (2011). Lateral organization of the postsynaptic density. Mol. Cell. Neurosci. *48*, 321–331.

Naisbitt, S., Kim, E., Tu, J.C., Xiao, B., Sala, C., Valtschanoff, J., Weinberg, R.J., Worley, P.F., and Sheng, M. (1999). Shank, a novel family of postsynaptic density proteins that binds to the NMDA receptor/PSD-95/GKAP complex and cortactin. Neuron *23*, 569–582.

Park, M., Salgado, J.M., Ostroff, L., Helton, T.D., Robinson, C.G., Harris, K.M., and Ehlers, M.D. (2006). Plasticity-induced growth of dendritic spines by exocytic trafficking from recycling endosomes. Neuron *52*, 817–830.

Park, H., Li, Y., and Tsien, R.W. (2012). Influence of synaptic vesicle position on release probability and exocytotic fusion mode. Science *335*, 1362–1366.

Penzes, P., Cahill, M.E., Jones, K.A., VanLeeuwen, J.E., and Woolfrey, K.M. (2011). Dendritic spine pathology in neuropsychiatric disorders. Nat. Neurosci. *14*, 285–293.

Raghavachari, S., and Lisman, J.E. (2004). Properties of quantal transmission at CA1 synapses. J. Neurophysiol. *92*, 2456–2467.

Ripley, B., Otto, S., Tiglio, K., Williams, M.E., and Ghosh, A. (2011). Regulation of synaptic stability by AMPA receptor reverse signaling. Proc. Natl. Acad. Sci. USA *108*, 367–372.

Saglietti, L., Dequidt, C., Kamieniarz, K., Rousset, M.C., Valnegri, P., Thoumine, O., Beretta, F., Fagni, L., Choquet, D., Sala, C., et al. (2007). Extracellular interactions between GluR2 and N-cadherin in spine regulation. Neuron *54*, 461–477.

Santamaria, F., Gonzalez, J., Augustine, G.J., and Raghavachari, S. (2010). Quantifying the effects of elastic collisions and non-covalent binding on glutamate receptor trafficking in the post-synaptic density. PLoS Comput. Biol. *6*, e1000780.

Santucci, D.M., and Raghavachari, S. (2008). The effects of NR2 subunit-dependent NMDA receptor kinetics on synaptic transmission and CaMKII activation. PLoS Comput. Biol. *4*, e1000208.

Schikorski, T., and Stevens, C.F. (1997). Quantitative ultrastructural analysis of hippocampal excitatory synapses. J. Neurosci. *17*, 5858–5867.

Sheng, M., and Hoogenraad, C.C. (2007). The postsynaptic architecture of excitatory synapses: a more quantitative view. Annu. Rev. Biochem. *76*, 823–847.

Shi, S., Hayashi, Y., Esteban, J.A., and Malinow, R. (2001). Subunit-specific rules governing AMPA receptor trafficking to synapses in hippocampal pyramidal neurons. Cell *105*, 331–343.

Shinohara, Y., Hirase, H., Watanabe, M., Itakura, M., Takahashi, M., and Shigemoto, R. (2008). Left-right asymmetry of the hippocampal synapses with differential subunit allocation of glutamate receptors. Proc. Natl. Acad. Sci. USA *105*, 19498–19503.

Steiner, P., Higley, M.J., Xu, W., Czervionke, B.L., Malenka, R.C., and Sabatini, B.L. (2008). Destabilization of the postsynaptic density by PSD-95 serine 73 phosphorylation inhibits spine growth and synaptic plasticity. Neuron *60*, 788–802.

Sturgill, J.F., Steiner, P., Czervionke, B.L., and Sabatini, B.L. (2009). Distinct domains within PSD-95 mediate synaptic incorporation, stabilization, and activity-dependent trafficking. J. Neurosci. *29*, 12845–12854.

Sugiyama, Y., Kawabata, I., Sobue, K., and Okabe, S. (2005). Determination of absolute protein numbers in single synapses by a GFP-based calibration technique. Nat. Methods *2*, 677–684.

Swulius, M.T., Kubota, Y., Forest, A., and Waxham, M.N. (2010). Structure and composition of the postsynaptic density during development. J. Comp. Neurol. *518*, 4243–4260.

Ting, J.T., Peça, J., and Feng, G. (2012). Functional consequences of mutations in postsynaptic scaffolding proteins and relevance to psychiatric disorders. Annu. Rev. Neurosci. *35*, 49–71.

Urban, N.T., Willig, K.I., Hell, S.W., and Nägerl, U.V. (2011). STED nanoscopy of actin dynamics in synapses deep inside living brain slices. Biophys. J. *101*, 1277–1284.

Valtschanoff, J.G., and Weinberg, R.J. (2001). Laminar organization of the NMDA receptor complex within the postsynaptic density. J. Neurosci. *21*, 1211–1217.

Xu, W., Schlüter, O.M., Steiner, P., Czervionke, B.L., Sabatini, B., and Malenka, R.C. (2008). Molecular dissociation of the role of PSD-95 in regulating synaptic strength and LTD. Neuron *57*, 248–262.